Heliyon 6 (2020) e05099

Contents lists available at ScienceDirect

Heliyon

journal homepage: www.cell.com/heliyon

Research article

Development of multi-product calibration models of various root and tuber powders by fourier transform near infra-red (FT-NIR) spectroscopy for the quantification of polysaccharide contents

Rudiati Evi Masithoh [a,*], Santosh Lohumi [b], Won-Seob Yoon [b], Hanim Z. Amanah [a,b], Byoung-Kwan Cho [b]

[a] Department of Agricultural and Biosystems Engineering, Faculty of Agricultural Technology, Universitas Gadjah Mada, Yogyakarta, 55281, Indonesia
[b] Department of Biosystems Machinery Engineering, College of Agricultural and Life Science, Chungnam National University, 99 Daehak-ro, Yuseoung-gu, Daejeon, 305-764, Republic of Korea

ARTICLE INFO

Keywords:
FT-NIR
PLS
PCA
Amylose
Starch
Cellulose
Engineering
Chemistry
Food science
Food analysis
Food safety

ABSTRACT

The objective of this study was to quantify the chemical content of multiple products using one single calibration model. This study involved seven tuber and root powders from arrowroot, *Canna edulis*, cassava, taro, as well as purple, yellow, and white sweet potato, for partial least square (PLS) regression to predict polysaccharide contents (i.e., amylose, starch, and cellulose). The developed PLS models showed acceptable results, with R_c^2 of 0.9, 0.95, and 0.85 and SEC of 2.7%, 3.33%, and 3.22%, for amylose, starch, and cellulose, respectively. The models also successfully predicted polysaccharide contents with R_p^2 of 0.89, 0.95, and 0.79; SEP of 2.83%, 3.33%, and 3.55%; and RPD of 3.02, 4.47, and 2.18 for amylose, starch, and cellulose, respectively. These results showed the potential of Fourier transform near-infrared spectroscopy to quantify the chemical composition of multiple products instead of using one individual model.

1. Introduction

Root and tuber crops are abundant in tropical countries and commonly consumed as flesh or powder products. Among those crops are cassava, potato, sweet potato, taro, arrowroot, and *Canna*. These crops are rich sources of carbohydrates and contain high levels of polysaccharides. Polysaccharides mainly contain cellulose as a texture enhancer to stimulate digestive enzyme (Kumar et al., 2012) and starch as a major source of carbohydrate (Yong et al., 2018) to provide energy. In powder form, roots, and tubers can be used as alternate powders made of grains or wheat in food production. As opposed to grains or wheat, those crops contain high amounts of resistant starch, which can improve the digestive system (Demartino and Cockburn, 2020). Moreover, the crops contain low levels of gluten (Food and Agriculture Organization (FAO), 1990), lowering the incidence of celiac disease and harmful immune responses caused by wheat consumption (Scherf et al., 2016).

The determination of polysaccharide contents is usually carried out by chemical analysis (Cai et al., 2014; Zhao et al., 2018), which requires intense work and relatively expensive analytical instruments. Therefore, the conventional method is difficult to use with large samples and routine analysis. Near-infrared (NIR) spectroscopy covers electromagnetic radiation in NIR regions at 14000–4000 cm^{-1}, and it is becoming popular for qualitative and quantitative food analyses. The spectrum in the NIR region contains information about the overtone and combination of fundamental vibrations useful for the identification of the interaction of molecules and chemical groups (Shi et al., 2019). Amylose is a type of starch that comprises a linear polymer of α-D-glucose units, which are connected by α-1,4 glycosidic bonds (Egharevba, 2019). Amylose is written as $[C_6H_{10}O_5]_n$, while cellulose is a polysaccharide composed of a linear chain of β-linked D-glucose units in fiber form. Given that C–H and O–H dominate the spectrum in those compounds, their functional groups can be easily analyzed by NIR spectroscopy.

Several studies utilized NIR spectroscopy for quality analysis of intact fruits (Jamshidi et al., 2012; Zhang et al., 2019), grains (Bagchi et al., 2016; Erkinbaev et al., 2017), liquids (de Sousa Marques et al., 2013; Masithoh et al., 2016), or for the determination of adulteration (Chen

* Corresponding author.
E-mail address: evi@ugm.ac.id (R.E. Masithoh).

https://doi.org/10.1016/j.heliyon.2020.e05099
Received 29 May 2020; Received in revised form 13 July 2020; Accepted 24 September 2020

Table 1. Mean and standard of deviation of cellulose, starch, and amylose of root and tuber powders.

Samples	Cellulose (%)	Starch (%)	Amylose (%)
Canna edulis	42.50 ± 4.17^{c}	43.14 ± 2.25^{f}	43.26 ± 2.13^{e}
Arrowroot	35.76 ± 6.44^{b}	38.87 ± 9.37^{e}	43.59 ± 2.63^{e}
Modified cassava	48.71 ± 1.52^{d}	18.05 ± 3.80^{c}	33.68 ± 1.84^{d}
Taro	25.02 ± 4.50^{a}	22.00 ± 4.39^{d}	24.29 ± 4.16^{b}
Purple sweet potato	41.36 ± 8.69^{c}	8.91 ± 2.45^{a}	26.02 ± 3.09^{b}
White sweet potato	38.91 ± 1.63^{bc}	12.40 ± 2.40^{b}	28.19 ± 2.55^{c}
Yellow sweet potato	39.97 ± 2.78^{c}	5.66 ± 0.97^{a}	20.99 ± 1.64a
All samples	38.89 ± 8.31	21.29 ± 14.22	31.43 ± 8.82

$^{a–f}$ Means followed by different letters in each column are significantly different among different types of flours ($p < 0.05$).

et al., 2019; Masithoh et al., 2020). NIR spectroscopy has also been widely used to determine quality parameters of several crops (Magwaza et al., 2016; Zhang et al., 2019). However, not many studies have examined roots and tubers. Several research groups studied tubers and roots (Ding et al., 2015; Lebot et al., 2009), but they used single crops in developing a calibration model to increase costs if several crops are necessary. Although the calibration model using multiple products was developed by Rambo et al. (2016) using banana, coffee and coconut samples, the application for multiple products of powders made of roots and tubers has not yet been conducted. Therefore, this study aimed to develop calibration models by using various root and tuber powders based on Fourier transform (FT)-NIR spectroscopy to determine their polysaccharide contents in terms of cellulose, starch, and amylose.

2. Material and methods

2.1. Sample

Tuber powders used in this study were made of seven crops, namely, arrowroot (*Maranta arundinacea*), canna edulis (*Canna indica*), purple, yellow, and white colour sweet potato (*Ipomoea batatas*), taro (*Colocasia esculenta*), and cassava (*Manihot esculenta*). For cassava, it was in the form of modified cassava flour. The samples were purchased from ten different sellers in Indonesia to obtain large varieties of samples. Of each crop, ten samples were obtained from ten different farmers, resulting in 70 sets of samples. For every set, three samples were utilized for spectral analysis for a total of 210 spectral data. All samples were dried in a 70 °C dryer for 1 day to eliminate moisture, which may affect the spectra, and sieved using a 212 μm sieve to obtain particles of uniform size. Water content of all samples were 8.24–18.64%.

2.2. FT-NIR spectra measurement

The spectra of 210 samples in reflectance mode were acquired using an FT-NIR spectrophotometer (Antaris II FT-NIR analyzer, Thermo Scientific Co., Waltham, MA, USA) with an InGaAs detector. Each sample was scanned for 32 scans at the range of 10,000–4000 cm^{-1} with 4 cm^{-1} intervals. A background scan was frequently conducted with a golden slit before acquiring the spectrum of each sample.

2.3. Chemical analysis

Cellulose determination. Cellulose was determined by modification of Eveleigh et al. (2009) method. After distillation using free sugar, 50 mL of enzyme cellulase (CTec2, Novozyme, DNK) and hemicellulase (Viscozyme, Novozyme, DNK) were added to yield 1 mL. The reaction was performed at 150 rpm, 40 °C, and 24 h using a shaking water bath. After vortexing, 1 mL of supernatant was obtained from the centrifuge (13,000 rpm, 4 °C, 10 min). After washing with 1 mL of distilled water for 30 s and another round of vortexing, the supernatant was acquired by centrifugation. About 3 mL of the supernatant, 100 μL of the sample, 200 μL of distilled water, and 900 μL of dinitrosalicylic acid (DNS) solution were added to a 1.5 mL tube. The sample tubes were allowed to react in boiling water for 5 min and cooled in ice for 15 min. Absorbance was measured at 575 nm with a microplate spectrophotometer. Cellulose content was presented in percentage (%).

Starch determination. Starch was determined by modification of Mccleary et al. (2019) method. After the cellulose assay, 1 mL of α-amylase (Termamyl, Novozyme, DNK) enzyme diluted with a factor of 50 was prepared with 50 mM sodium acetate buffer and 50 mM acetic acid buffer. The mixture was then reacted at 95 °C for 2 h. After the reaction, 900 μL of glucoamylase diluted in 100 μL of supernatant pH 4.3

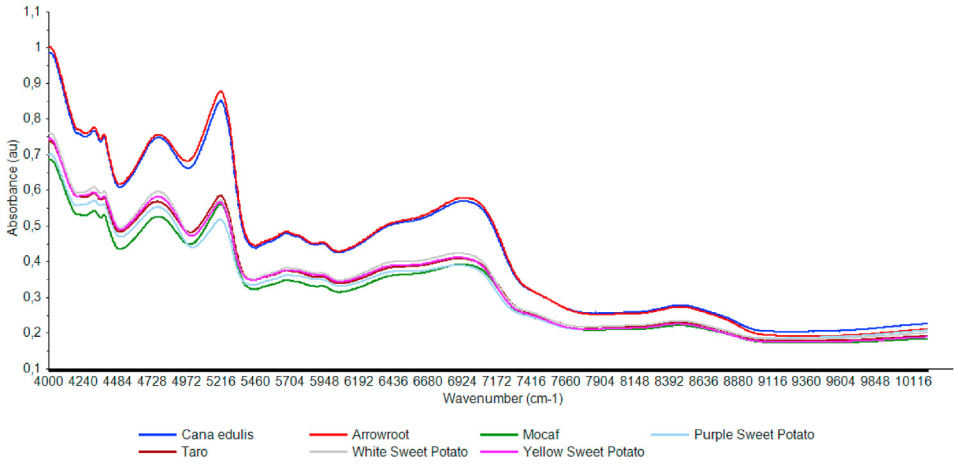

Figure 1. Original spectra of *Canna edulis*, arrowroot, modified cassava (mocaf), purple sweet potato, taro, white sweet potato, and yellow sweet potato powder in the region of 4000–10,000 cm^{-1}

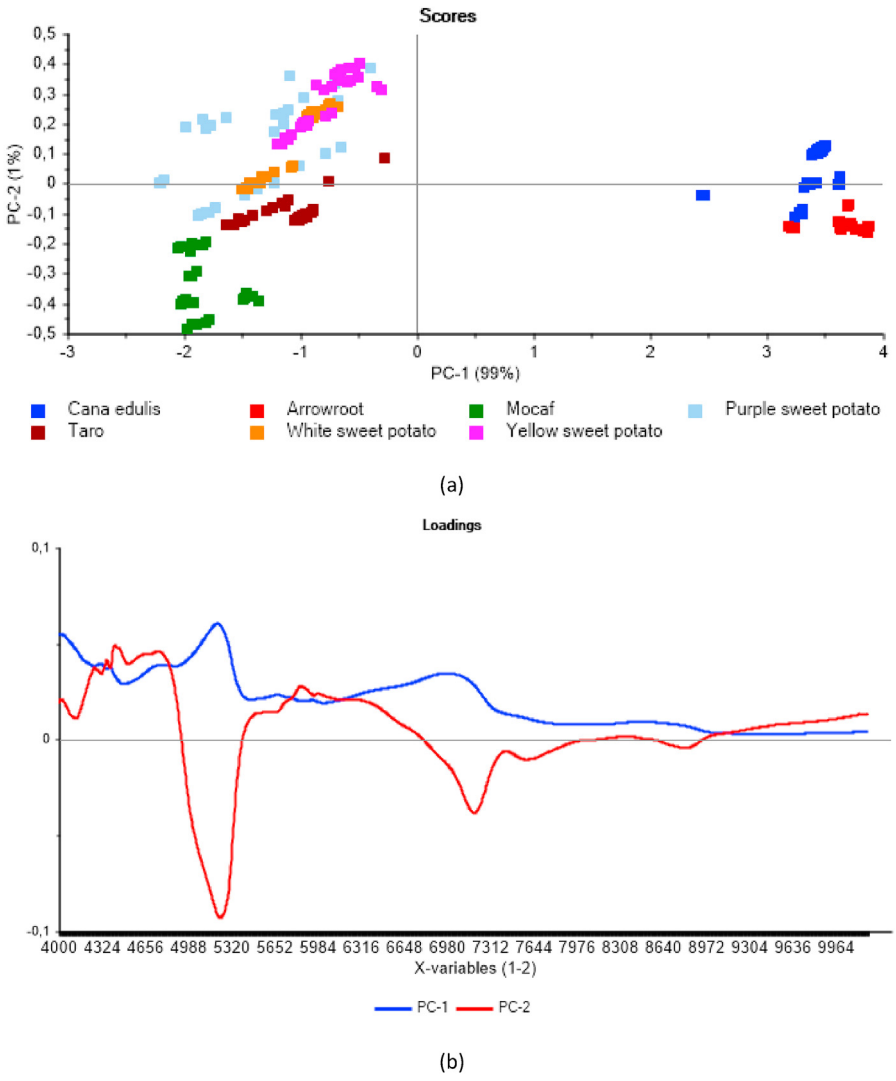

Figure 2. (a) PCA score plot and (b) loading values of PCs of original spectra.

buffer was prepared with 50 mM sodium acetate buffer. Subsequently, 50 mM acetic acid buffer was added and reacted at 55 °C for 2 days. About 1 mL of GOPOD solution was added to 100 μL of the sample, vortexed, and reacted at 40 °C for 20 min. The sample was then stabilized to room temperature by using ice. Absorbance was measured at 510 nm with a spectrophotometer. Starch content was presented in percentage (%).

Amylose was determined by modification of method. Samples (0.3–0.4 g) in a 50 mL tube were weighed, added with 5 mL of toluene, and subjected to O/N shaking at 25 °C and 130 rpm. Another toluene wash was conducted prior to protein and lipid removal. Toluene was then completely removed using SpeedVac. Samples of 0.1 g were placed into a 50 mL tube, dissolved with 90% DMSO in 50 mM pH 5.0 sodium acetate buffer, and melted completely with 20 min of boiling and 20 min of sonication. About 1 mL of Lugol's solution diluted 10-fold to 100 μL was added to the sample and vortexed. Finally, the sample was diluted in Lugol's solution (50 mM pH 5.0 sodium acetate buffer). Absorption of the amylose complex was measured at 620 nm with a spectrophotometer. Amylose content was presented in percentage (%).

2.4. Spectral analysis

All spectra collected using Thermo Scientific™ OMNIC™ Series Software were then transformed to MS Excel® 2013 and Unscrambler®X (Version 10.5.1, CAMO Software, Norway) for spectral pre-processing and chemometric analysis. Two chemometric techniques were used: principal component analysis (PCA) and partial least-squares regression (PLSR). PCA was used for dimension reduction and data visualization of samples. PLSR was applied to predict the starch, cellulose, and amylose contents of tuber samples. To develop the PLSR model, the FT-NIR spectra were pre-processed through smoothing, baseline corrections, normalization (mean, max, and range), Standard Normal Variate (SNV), and Multiplicative Scatter Correction (MSC) methods. Of 210 spectra data, 50% and 50% of the data were used for calibration and prediction, respectively. Full-cross validation was carried out to develop a calibration model using PLSR. The best model was selected based on five statistical methods, i.e., coefficient of determination (R^2) of calibration (R^2_c), standard error of calibration (SEC), determination of prediction (R^2_p),

Table 2. Calibration and predicted results of partial least square regression (PLSR) for *Canna edulis*, arrowroot, modified cassava, taro, purple sweet potato, white sweet potato, and yellow sweet potato powders by using several pre-processed methods.

Pre-processing		ORI	SM	MN	RN	MAXN	BS	SNV	MSC
Amylose	R_c^2	0.9	0.9	0.9	0.9	0.9	0.89	0.9	0.9
	SEC	2.71	2.72	2.75	2.76	2.72	2.78	2.7	2.72
	R_p^2	0.89	0.8	0.89	0.89	0.89	0.89	0.89	0.89
	SEP	2.84	2.89	2.89	2.88	2.89	2.92	2.83	2.86
	RPD	3.02	2.24	3.02	3.02	3.02	3.02	3.02	3.02
Starch	R_c^2	0.95	0.95	0.92	0.91	0.91	0.95	0.95	0.95
	SEC	3.33	3.33	4.14	4.27	4.27	3.38	3.32	3.3
	R_p^2	0.93	0.95	0.91	0.9	0.90	0.93	0.93	0.93
	SEP	3.89	3.33	4.38	4.47	4.47	3.94	3.83	3.82
	RPD	3.78	4.47	3.33	3.16	3.16	3.78	3.78	3.78
Cellulose	R_c^2	0.76	0.75	0.83	0.83	0.82	0.83	0.85	0.85
	SEC	4.1	4.19	3.47	3.43	3.55	3.41	3.22	3.31
	R_p^2	0.71	NA	0.77	0.77	0.77	0.75	0.79	0.78
	SEP	4.08	6.4	3.76	3.77	3.76	3.93	3.55	3.64
	RPD	1.86	NA	2.09	2.09	2.09	2.00	2.18	2.13

Note: ORI = original; SM = smoothing; MN = mean normalization; RN = range normalization; MAXN = maximum normalization; BS = baseline correction; SNV = standard normal variate; MSC = multiplicative scatter correction (MSC); R_c^2 = coefficient of determination of calibration; R_p^2 = coefficient of determination of prediction; SEC = standard error of calibration; SEP = standard error of prediction; RPD = ratio of prediction to deviation.

standard error of prediction (SEP), and ratio of prediction to deviation (RPD) (Li et al., 2015).

3. Results and discussion

3.1. Data exploration

Table 1 shows the mean and standard deviation of cellulose, starch, and amylose in root and tuber powders as determined by wet chemical analysis. The highest and lowest cellulose contents belonged to modified cassava (MC) and taro (TR) powder, respectively. *C. edulis* powder had the highest starch content, while yellow sweet potato powder had the lowest starch content. In general, all family of sweet potatoes (white, yellow, and purple) had lower starch contents compared with other crops. These findings were similar to a study conducted by (Lebot, 2010) on cassava and sweet potato crops. Meanwhile, the highest amylose contents were found in arrowroot and *C. edulis* powders, while the lowest was observed in yellow sweet potato powder.

Original spectra of samples are presented in Figure 1, which showed a similar trend of all root and tuber powders in the wavenumber range of 4000–10,000 cm^{-1}. However, the spectra of *C. edulis* and arrowroot powders were indicated by higher relative absorbance compared with those of other powders. Significant peaks on the FT-NIR spectra were observed, such as the highest absorption band at 5184 cm^{-1}, which was attributed to OH stretching and bending in amylose (Sampaio et al., 2018). Other peaks were found at 4280 cm^{-1}, which was due to CH stretching and deformation in polysaccharides (Li et al., 2015), and at 5102 cm^{-1}, which was the result of OH stretching or bending in starch (Aenugu et al., 2011). Another absorption peak at 4860 cm^{-1} was caused by N–H stretching in protein; a weak but broad absorption peak was observed at around 8620 cm^{-1}, which was attributed to CO stretching in starch (Williams, 2001).

3.2. Principal component analysis (PCA)

Given that variable data resulting from FT-NIR spectroscopy are large, data without missing information can be visualized by PCA (Guillén--Casla et al., 2011). By using the original spectra shown in Figure 2(a), all samples could be explained by PC 1 and PC 2 with 99% and 1% of total variance, respectively. White, purple, and yellow sweet potato were grouped together and presented positive values in PC 2. Those powders also demonstrated negative values in PC 1, along with mocaf and taro. Mocaf and taro powders exhibited negative values of PC 2. Arrowroot and *C. edulis* had negative and positive values of PC 2, respectively.

Figure 2(b) shows the positive loadings of PC 1 around 5216 cm^{-1} for arrowroot and *C. edulis*; this peak was assigned to the OH first stretching overtone due to the presence of amylose. These findings were supported by the amylose content of arrowroot and *C. edulis*, which were similar and higher compared with other powders (see Table 1). The positive loadings of PC 1 at around 6968 cm^{-1} corresponded to C–H stretching and represented the starch content (Lohumi et al., 2014). In the present study, arrowroot and *C. edulis* also had a higher starch content than other powders. Tuber and root crops are high in fiber (Chandrasekara and Kumar, 2016), including cellulose, which was indicated in the peak at around 4405 cm^{-1} due to OH or CO stretching (Aenugu et al., 2011). In Figure 2(b), the high cellulose contents of all sweet potato and *C. edulis* samples (Table 1) were shown by the positive loadings of PC 2.

3.3. PLSR for quantification of cellulose, amylose, and starch contents

PLSR was used to relate the FT-NIR instrument variables to the dependent variables. In this study, the dependent variables were amylose, cellulose, and starch contents of *C. edulis*, arrowroot, MC, taro, purple sweet potato, white sweet potato, and yellow sweet potato powders. A single calibration model was obtained for the determination of cellulose of all powders made of seven tubers and root crops. Two other calibration models were used to determine the amylose and starch contents. Several methods can be used to select the best calibration model that yields high accuracy. In general, the models are assessed by statistics indicators such as R_c^2, SEC, R_p^2, SEP, and RPD (Li et al., 2015).

The PLSR models were developed using original and pre-processed spectra of samples from FT-NIR instrument. Results of PLS analysis are provided in Table 2, showing R^2, SEC, SEP, and RPD. R^2 indicates the variation percentage of Y variables (i.e., amylose, starch, and cellulose contents), which are accounted for by the X variables (absorbance). R^2 above 0.83 is usable with caution for most applications, while that above 0.92 is usable in most applications Standard error of calibration (SEC) and prediction (SEP) are the standard deviation of differences between

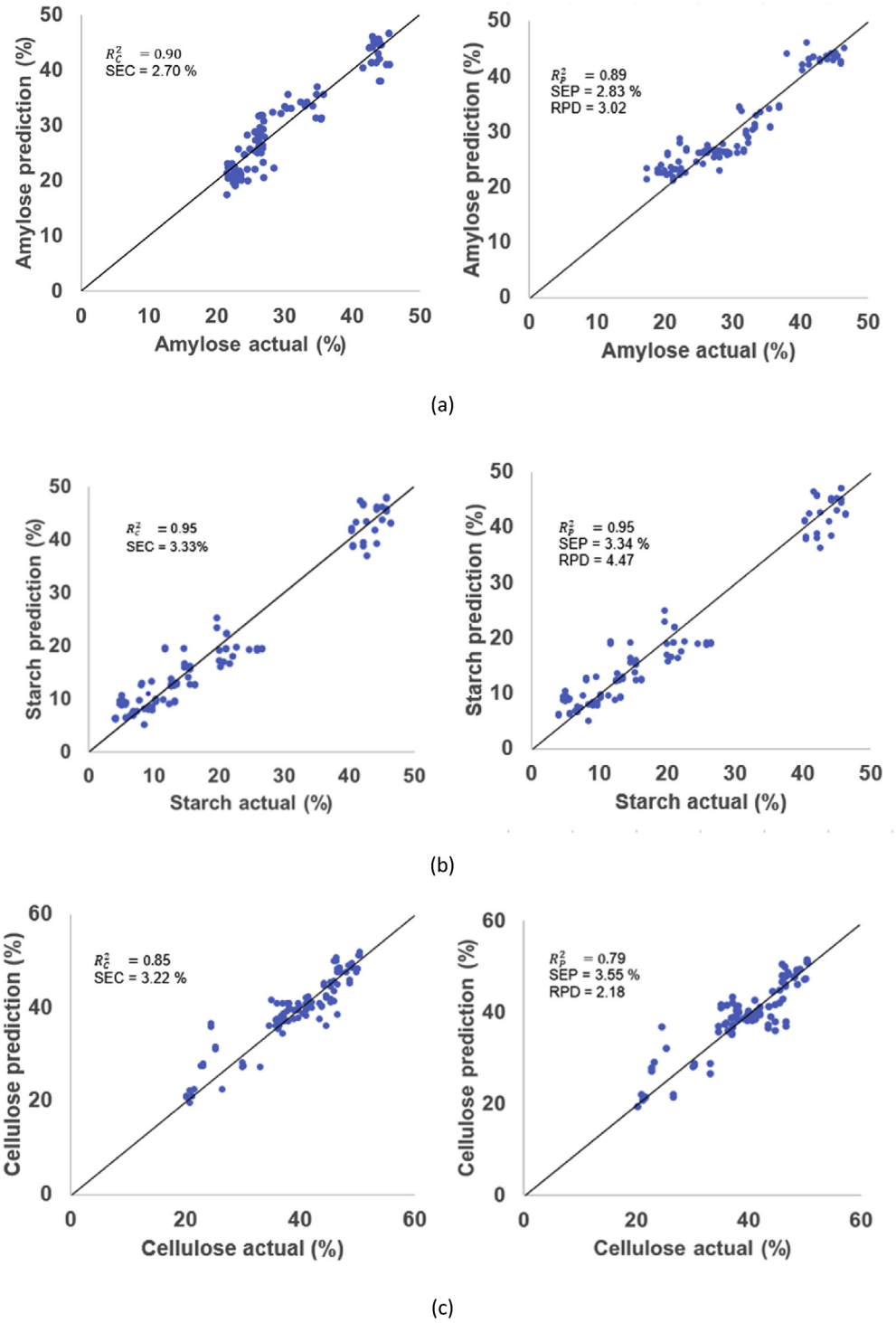

Figure 3. NIR scatter plots of calibration (left) and prediction (right) data sets of (a) amylose, (b) starch, and (c) cellulose showing R_c^2, SEC, R_p^2, SEP, and RPD values resulted from PLS regression.

NIR and reference samples in the calibration and prediction sample sets. A good model has low SEC and SEP. RPD measured the accuracy of model prediction; values of 1.5–2.0, 2.0–2.5, and above 2.5–3.0 can provide rough screening, estimated quantitative screening, and excellent screening, respectively (Lebot et al., 2009).

As shown in Table 2, the PLS calibration models developed by using original and pre-processed spectra resulted in R_c^2 of 0.75–0.85, 0.8–0.9, and 0.91–0.95, for cellulose, amylose, and starch, respectively. SEC for cellulose, amylose, and starch was in the range of 3.22–4.19 (%), 2.7–2.79 (%), and 2.95–4.27 (%), respectively. R_p^2, SEP, and RPD were obtained from predicted data, which were calculated using the calibration models. The PLS calibration models could predict cellulose, amylose, and starch contents with R_p^2 of 0.71–0.79, 0.8–0.89, and 0.90–0.95, as well as SEP of 3.55–6.4 (%), 2.83–2.89 (%), and 3.34–4.47 (%), respectively. Moreover, the model could predict cellulose, amylose, and starch contents with RPD of 1.86–2.18, 2.24–3.02, and 3.16–4.47, respectively.

The best calibration model for quantification of amylose with R_c^2 of 0.9 and SEC of 2.7% was achieved by applying the SNV method. The best calibration model for predicting the amylose content was obtained with

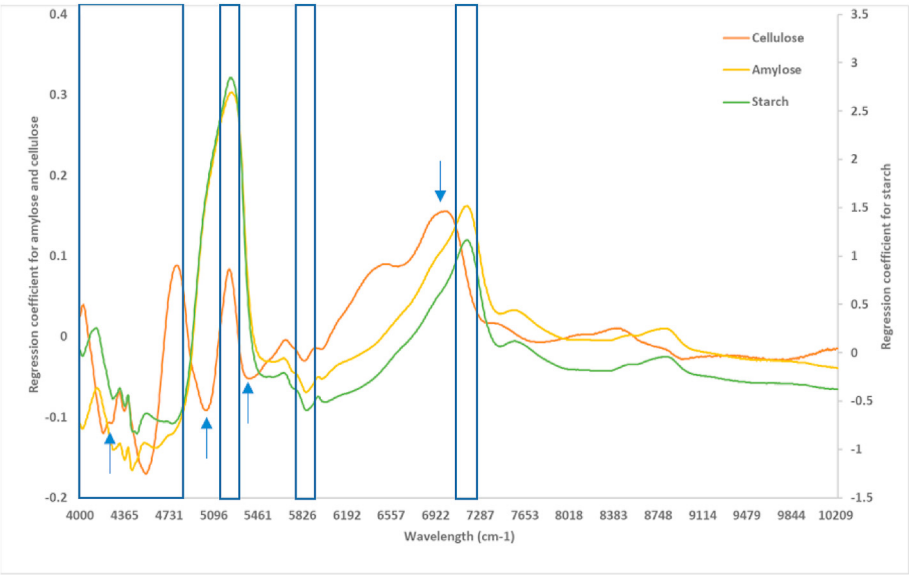

Figure 4. Regression coefficient (B) of PLSR using the SNV method for quantification of amylose and cellulose, as well as the smoothing method for quantification of starch.

one latent variable. The model was then applied to predict the amylose content, which resulted in R_p^2 of 0.89, SEP of 2.83%, and RPD of 3.02. Scatter plot using calibration and prediction data sets for amylose quantification was shown in Figure 3(a). For the quantification of the starch content, smoothing was applied to raw spectra, which resulted in R_c^2 of 0.95 and SEC of 3.33%. The model could predict the starch content with R_p^2 of 0.95, SEP of 3.34%, and RPD of 4.47. Results of calibration and prediction models for starch were illustrated as scatter plots in Figure 3(b). The calibration model for predicting the cellulose content with the highest R_c^2 of 0.85 and the lowest SEC of 3.22% was obtained by applying SNV (Table 2). By using predicted samples, the model could predict the cellulose content with R_p^2 of 0.79, SEP of 3.55%, and RPD of 2.18. Figure 3(c) showed scatter plots of calibration and prediction models for cellulose quantification.

Those obtained statistical values were acceptable (Williams, 2001), which implied that the models for quantifying amylose, starch, and cellulose in this study were sufficient for agricultural applications. Other studies obtained R^2 of 0.97 and 0.93 for amylose and total starch of pea flour (Zeng and Chen, 2018), coefficient correlation (R) of 0.94 for amylose in rice (Sampaio et al., 2018), R^2 of 0.94 of starch in sweet potato (Katayama et al., 1996), R^2 of 0.93 in Moso bamboo (Li et al., 2015), and R^2 of 0.82 for zucchini (Pomares-viciana et al., 2018). However, those findings used a single product for each analysis.

The PLS loadings or coefficients of regression were used to interpret which bands were highly correlated with the contents of amylose, starch, and cellulose. Figure 4 shows the regression coefficients for predicting the contents of amylose, starch, and cellulose of tuber and root crops, i.e., arrowroot, *C. edulis*, cassava (in the form of MC powder), taro, as well as purple, yellow, and white sweet potato. The trends of the three spectra were similar because they were carbohydrates, but starch showed higher absorbance values than amylose and cellulose. Several peaks similarly owned by those polysaccharides were marked with rectangles, such as those at 4036, 4788, 5216, and 5860 cm^{-1}. Another peak was detected at around 7196 cm^{-1} for amylose and starch, but a slight shift to 7020 cm^{-1} was noted for cellulose.

Both amylose and starch have very similar shapes, but starch has a higher absorbance intensity across the spectral region than amylose. This difference is due to the fact that both starch and amylose are polysaccharides made up of glucose units (Egharevba, 2019). Significant peaks with relatively high absolute regression coefficient values for amylose and starch are portrayed in Figure 4 at 4428, 5240, and 7168 cm^{-1}; these peaks corresponded to OH stretching/CO stretching, OH stretching first overtone, and CH combination (Shenk et al., 2008). (Xie et al., 2014) and (Zeng and Chen, 2018) marked significant bands for the amylose determination of rice flour at 6493 and 8143 cm^{-1} and pea flour at 7012 cm^{-1}. Similar peaks around 4000–7000 cm^{-1} were found for kudzu, maize, sweet potato, cassava, and potato starch (Xu et al., 2015). Peaks around 4073, 4325, and 7042 cm^{-1} corresponding to CH stretching and deformation vibrations and OH first overtone in starch were observed by (Lohumi et al., 2014).

Cellulose is a polysaccharide with extended structure linear polymer of glucose allowing hydrogen bonding between OH groups on nearby chains to group closely into fibers exhibiting little interaction with water or other solvents (LibreTexts, 2019). In Figure 4, several prominent peaks of the cellulose spectra (indicated by arrows) were observed at 4260 (CH_2 symmetrical stretching and = CH_2 deformation), 5036 (OH stretching/OH bending), 5404 (CO stretch second overtone), and 7020 cm^{-1} (OH first overtone) (Shenk et al., 2008).

4. Conclusion

This study demonstrated that FT-NIR spectroscopy can be used to quantify the amylose, starch, and cellulose contents of seven tuber and crop powder with high degree accuracy. The calibration models show R_c^2 and SEC of 0.9 and 2.7% for amylose, 0.96 and 2.95% for starch, as well as 0.85 and 3.22% for cellulose, respectively. When applied to predict polysaccharide content, the models result in R_p^2 of 0.89, SEP of 2.83%, and RPD of 3.02 for amylose, R_p^2 of 0.96, SEP of 2.95%, and RPD of 5.00 for starch, as well as R_p^2 of 0.79, SEP of 3.55%, and RPD of 2.18 for cellulose. Those statistical values indicate that the developed calibration models can be used to predict chemical content of multiple crops in powder form. Therefore, the models can reduce the cost and time compared to single use analysis.

Declarations

Author contribution statement

Rudiati Evi Masithoh: Conceived and designed the experiments; Performed the experiments; Analyzed and interpreted the data; Contributed materials, analysis tools or data; Wrote the paper.

Santosh Lohumi: Analyzed and interpreted the data

Won-Seob Yoon: Performed the experiments.

Hanim Z Amanah: Performed the experiments.

Byoung-Kwan Cho: Contributed reagents, materials, analysis tools or data; Reviewed the paper.

Funding statement

This research was supported by a grant from the Next-Generation BioGreen 21 Program (No. PJ01311303), Rural Development Administration, Republic of Korea.

Competing interest statement

The authors declare no conflict of interest.

Additional information

No additional information is available for this paper.

References

Aenugu, H.P.R., Sathis Kumar, D., Srisudharson, Parthiban, N., Ghosh, S.S., Banji, D., 2011. Near infra red spectroscopy- an overview. Int. J. Chem. Res. 3, 825–836.

Bagchi, T.B., Sharma, S., Chattopadhyay, K., 2016. Development of NIRS models to predict protein and amylose content of brown rice and proximate compositions of rice bran. Food Chem. 191, 21–27.

Cai, J., Cai, C., Man, J., Zhou, W., Wei, C., 2014. Structural and functional properties of C-type starches. Carbohydr. Polym. 101, 289–300.

Chandrasekara, A., Kumar, T.J., 2016. Roots and tuber crops as functional foods: a review on phytochemical constituents and their potential health benefits. Int. J. Food Sci. 1–15, 2016.

Chen, H., Tan, C., Lin, Z., Li, H., 2019. Quantifying several adulterants of notoginseng powder by near-infrared spectroscopy and multivariate calibration. Spectrochim. Acta Part A Mol. Biomol. Spectrosc. 211, 280–286.

de Sousa Marques, A., Nicácio, J.T.N., Cidral, T.A., de Melo, M.C.N., De Lima, K.M.G., 2013. The use of near infrared spectroscopy and multivariate techniques to differentiate Escherichia coli and Salmonella Enteritidis inoculated into pulp juice. J. Microbiol. Methods 93, 90–94.

Demartino, P., Cockburn, D.W., 2020. ScienceDirect Resistant starch : impact on the gut microbiome and health. Curr. Opin. Biotechnol. 61, 66–71.

Ding, X., Ni, Y., Kokot, S., 2015. NIR spectroscopy and chemometrics for the discrimination of pure, powdered, purple sweet potatoes and their samples adulterated with the white sweet potato flour. Chemometr. Intell. Lab. Syst. 144, 17–23.

Egharevba, H.O., 2019. Chemical Properties of Starch and its Application in the Food Industry. IntechOpen, London.

Erkinbaev, C., Henderson, K., Paliwal, J., 2017. Discrimination of gluten-free oats from contaminants using near infrared hyperspectral imaging technique. Food Contr. 80, 197–203.

Eveleigh, D.E., Mandels, M., Andreotti, R., Roche, C., 2009. Measurement of saccharifying cellulase. Biotechnol. Biofuels 2, 21.

Food and Agriculture Organization (FAO), 1990. Roots, Tubers, Plantains and Bananas in Human Nutrition. Food and Nutrition Series, Rome, Italy.

Guillén-Casla, V., Rosales-Conrado, N., León-González, M.E., Pérez-Arribas, L.V., Polo-Díez, L.M., 2011. Principal component analysis (PCA) and multiple linear regression (MLR) statistical tools to evaluate the effect of E-beam irradiation on ready-to-eat food. J. Food Compos. Anal. 24, 456–464.

Jamshidi, B., Minaei, S., Mohajerani, E., Ghassemian, H., 2012. Reflectance Vis/NIR spectroscopy for nondestructive taste characterization of Valencia oranges. Comput. Electron. Agric. 85, 64–69.

Katayama, K., Komaki, K., Tamiya, S., 1996. Prediction of starch , moisture , and sugar in sweetpotato by near infrared transmittance. Hortscience 31, 1003–1006.

Kumar, V., Sinha, A.K., Makkar, H.P.S., De Boeck, G., 2012. Dietary Roles of Non-starch Polysachharides in Human Nutrition : A Review Dietary Roles of Non-starch Polysachharides in Human Nutrition: 8398.

Lebot, V., 2010. Tropical root and tuber crops. In: Verheye, W.H. (Ed.), Soils, Plant Growth and Crop Production. EOLSS.

Lebot, V., Champagne, A., Malapa, R., Shiley, D., 2009. NIR determination of major constituents in tropical root and tuber crop flours. J. Agric. Food Chem. 57, 10539–10547.

Li, X., Sun, C., Zhou, B., He, Y., 2015. Determination of hemicellulose, cellulose and lignin in Moso bamboo by near infrared spectroscopy. Sci. Rep. 5, 1–11.

LibreTexts, 2019. Starch and Cellulose [WWW Document]. URL. https://chem.libretexts.org/link?30355.

Lohumi, S., Lee, S., Lee, W., Kim, M.S., Mo, C., Bae, H., Cho, B.K., 2014. Detection of starch adulteration in onion powder by FT-NIR and FT-IR spectroscopy. J. Agric. Food Chem. 62, 9246–9251.

Magwaza, L.S., Messo Naidoo, S.I., Laurie, S.M., Laing, M.D., Shimelis, H., 2016. Development of NIRS models for rapid quantification of protein content in sweetpotato [Ipomoea batatas (L.) LAM.]. LWT - Food Sci. Technol. (Lebensmittel-Wissenschaft -Technol.) 72, 63–70.

Masithoh, R., Haff, R., Kawano, S., 2016. Determination of soluble solids content and titratable acidity of intact fruit and juice of satsuma Mandarin using a hand-held near infrared instrument in transmittance mode. J. Near Infrared Spectrosc. 24, 83.

Masithoh, R.E., Amanah, H.Z., Cho, B.K., 2020. Application of Fourier Transform Near-Infrared (FT-NIR) and Fourier Transform Infrared (FT-IR) spectroscopy coupled with wavelength selection for fast discrimination of similar color of tuber flours. Indones. J. Chem. 20, 680.

Mccleary, B.V., Charmier, L.M.J., Mckie, V.A., 2019. Measurement of starch : critical evaluation of current methodology. Starch 1800146, 1–13.

Pomares-viciana, T., Martínez-valdivieso, D., Font, R., Gómez, P., Río-celestino, M., 2018. Characterisation and prediction of carbohydrate content in zucchini fruit using near infrared spectroscopy. J. Sci. Food Agric. 98, 1703–1711.

Rambo, M.K.D., Ferreira, M.M.C., Amorim, E.P., 2016. Multi-product calibration models using NIR spectroscopy. Chemometr. Intell. Lab. Syst. 151, 108–114.

Sampaio, P.S., Soares, A., Castanho, A., Almeida, A.S., Oliveira, J., Brites, C., 2018. Optimization of rice amylose determination by NIR-spectroscopy using PLS chemometrics algorithms. Food Chem. 242, 196–204.

Scherf, K.A., Koehler, P., Wieser, H., 2016. Gluten and wheat sensitivities - an overview. J. Cereal. Sci. 67, 2–11.

Shenk, J.S., Workman, J.J., Westerhaus, M.O., 2008. Application of NIR spectroscopy to agricultural products. In: Burns, D.A., Ciurczak, E.W. (Eds.), Handbook of Near-Infrared Analysis. CRC Press, Boca Raton.

Shi, H., Lei, Y., Louzada Prates, L., Yu, P., 2019. Evaluation of near-infrared (NIR) and Fourier transform mid-infrared (ATR-FT/MIR) spectroscopy techniques combined with chemometrics for the determination of crude protein and intestinal protein digestibility of wheat. Food Chem. 272, 507–513.

Williams, P.C., 2001. Implementation of near-infrared technology. In: Williams, P., Noris, K. (Eds.), Near-Infrared Technology in the Agricultural and Food Industries. The American Association of Cereal Chemist, Inc., Minnesota.

Xie, L.H., Tang, S.Q., Chen, N., Luo, J., Jiao, G.A., Shao, G.N., Wei, X.J., Hu, P.S., 2014. Optimisation of near-infrared reflectance model in measuring protein and amylose content of rice flour. Food Chem. 142, 92–100.

Xu, L., Shi, W., Cai, C.B., Zhong, W., Tu, K., 2015. Rapid and nondestructive detection of multiple adulterants in kudzu starch by near infrared (NIR) spectroscopy and chemometrics. LWT - Food Sci. Technol. (Lebensmittel-Wissenschaft -Technol.) 61, 590–595.

Yong, H., Wang, X., Sun, J., Fang, Y., Liu, J., Jin, C., 2018. Comparison of the structural characterization and physicochemical properties of starches from seven purple sweet potato varieties cultivated in China. Int. J. Biol. Macromol. 120, 1632–1638.

Zeng, L., Chen, C., 2018. Simultaneous estimation of amylose, resistant, and digestible starch in pea flour by visible and near-infrared reflectance spectroscopy. Int. J. Food Prop. 21, 1129–1137.

Zhang, D., Xu, Y., Huang, W., Tian, X., Xia, Y., Xu, L., Fan, S., 2019. Nondestructive measurement of soluble solids content in apple using near infrared hyperspectral imaging coupled with wavelength selection algorithm. Infrared Phys. Technol. 98, 297–304.

Zhao, X., Andersson, M., Andersson, R., 2018. Resistant starch and other dietary fiber components in tubers from a high-amylose potato. Food Chem. 251, 58–63.